nature neuroscience

SUPPLEMENTARY INFORMATION

https://doi.org/10.1038/s41593-019-0381-8

In the format provided by the authors and unedited.

Predictive and reactive reward signals conveyed by climbing fiber inputs to cerebellar Purkinje cells

Dimitar Kostadinov[1]*, Maxime Beau[1], Marta Blanco-Pozo[1,2] and Michael Häusser[1]*

[1]Wolfson Institute for Biomedical Research and Department of Neuroscience, Physiology and Pharmacology, University College London, London, UK. [2]Present address: Department of Experimental Psychology, University of Oxford, Oxford, UK. *e-mail: dimvladkost@gmail.com; m.hausser@ucl.ac.uk

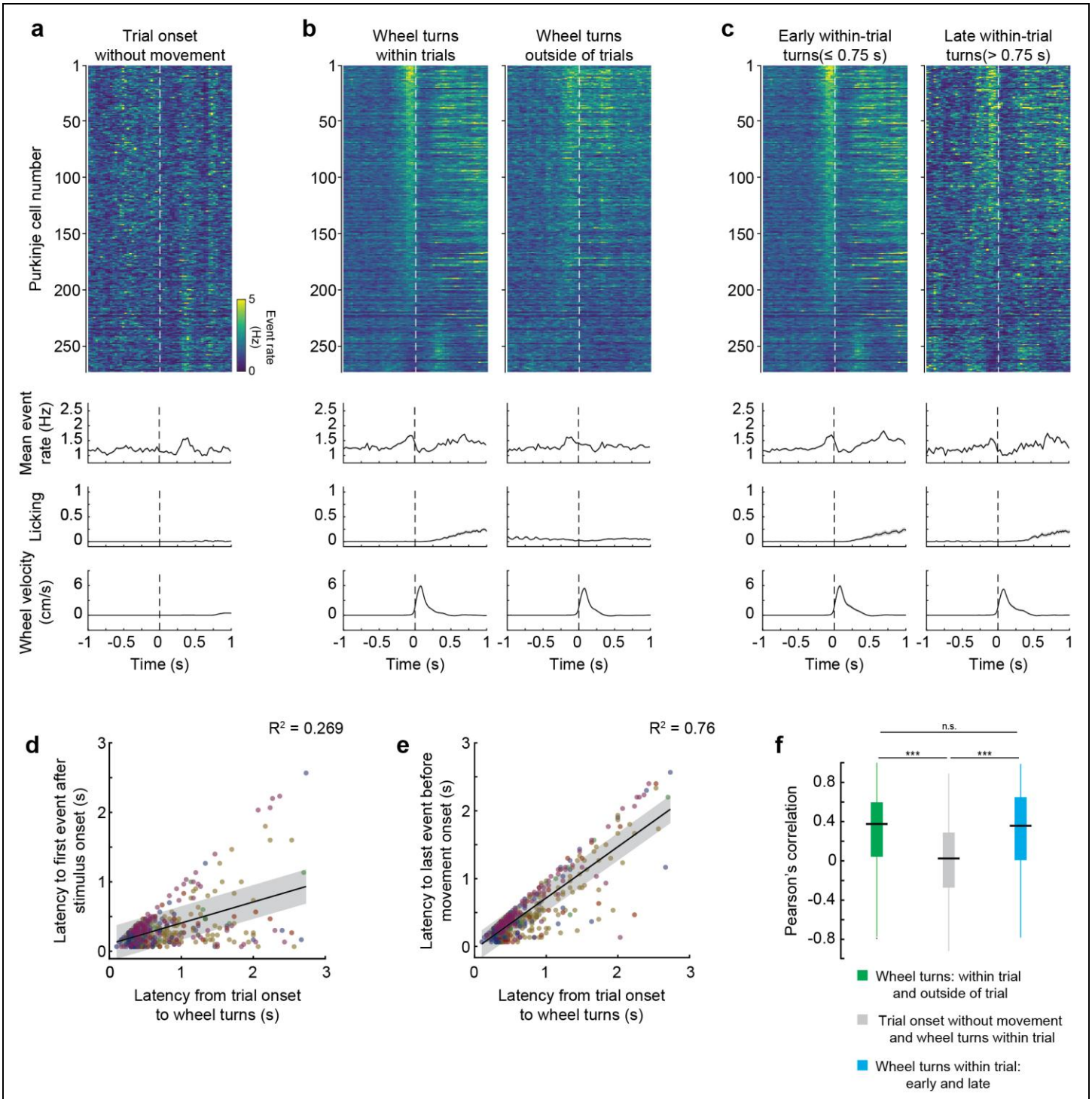

Supplementary Figure 1

Activity aligned to movement onset is preferentially related to movement and not to object appearance

a. Top: Events extracted from population two-photon calcium imaging of Purkinje cells during the behavioral task, expressed as a heatmap. Activity in an example session is aligned to object appearance (dashed line) on trials in which the mouse did not immediately turn the wheel (turn latency > 0.75 s). Bottom: summary of activity and behavior for all sessions. N = 1101 neurons, 6 mice, 6 sessions

(1 session per mouse). Data are shown as mean ± s.e.m.

b. Top: Heatmap of activity in an example session aligned to wheel turns (dashed line) that occurred within a trial (left) or outside of a trial (right). Bottom: summary of activity and behavior for all sessions. N = 1101 neurons, 6 mice, 6 sessions (1 session per mouse). Data are shown as mean ± s.e.m.

c. Top: Heatmap of activity in an example session aligned to wheel turns (dashed line) that occurred early within a trial (turn latency ≤ 0.75 s) or late in a trial (turn latency > 0.75 s). Bottom: summary of activity and behavior for all sessions. N = 859 neurons, 5 mice, 5 sessions (1 session per mouse). Note that one session was excluded from these analyses because it only had 4 trials in which it initiated a movement with turn latency > 0.75 s. Data are shown as mean ± s.e.m.

d. Comparison of first significant population-wide event after object appearance (defined as the time points when the mean event rate for a field of view exceeded the mean + 2 s.d. of activity during the withhold period on each trial) to the reaction time of the mouse on each trial. Dots represent individual trials and dots of the same color represent individual sessions (one session per mouse). Black line and shaded bar represent linear fit and 95% confidence interval through all data points (linear regression, $p = 3x10^{-42}$). N = 594 trials, 6 mice, 6 sessions (1 session per mouse).

e. Same as panel **d** but for the last population-wide event before movement onset (linear regression, $p = 8x10^{-190}$).

f. Summary of Pearson's correlation coefficients of activity traces for individual neurons between wheel turns within trial and outside of trial (green bar, interval -300 to +300 ms relative to wheel movement, N = 1101 neurons, 6 mice, 6 sessions), between trial onsets without movement and wheel turns within a trial (gray bar, interval +100 to 700 ms for trial onset and -300 to +300 ms for wheel turns in order to align peaks of activity, N = 1101 neurons, 6 mice, 6 sessions), and between wheel turns that occurred early within a trial and movements that occurred late within a trial (blue bar, interval -300 to +300 ms relative to wheel movement, N = 859 neurons, 5 mice, 5 sessions). Intervals for correlation analysis were chosen to align the peaks of the responses for each condition. Data are shown as box plots: center line, median; box edges, interquartile ranges; whiskers, range without outliers (1.5 times the interquartile range from box edges); black points, outliers (Kruskal-Wallis test, H = 359, d.f. = 2, $p = 9x10^{-79}$, significance values for Bonferroni-corrected individual comparisons: wheel turns: within trial and outside of trial vs trial onset without movement and wheel turns within trial, $p = 7x10^{-63}$; wheel turns: within trial and outside of trial vs wheel turns within trial: early and late, p > 0.9; trial onset without movement and wheel turns within trial vs wheel turns within trial: early and late, $p = 1x10^{-54}$).

Statistics summary: n.s. = not significant, ***p < 0.001.

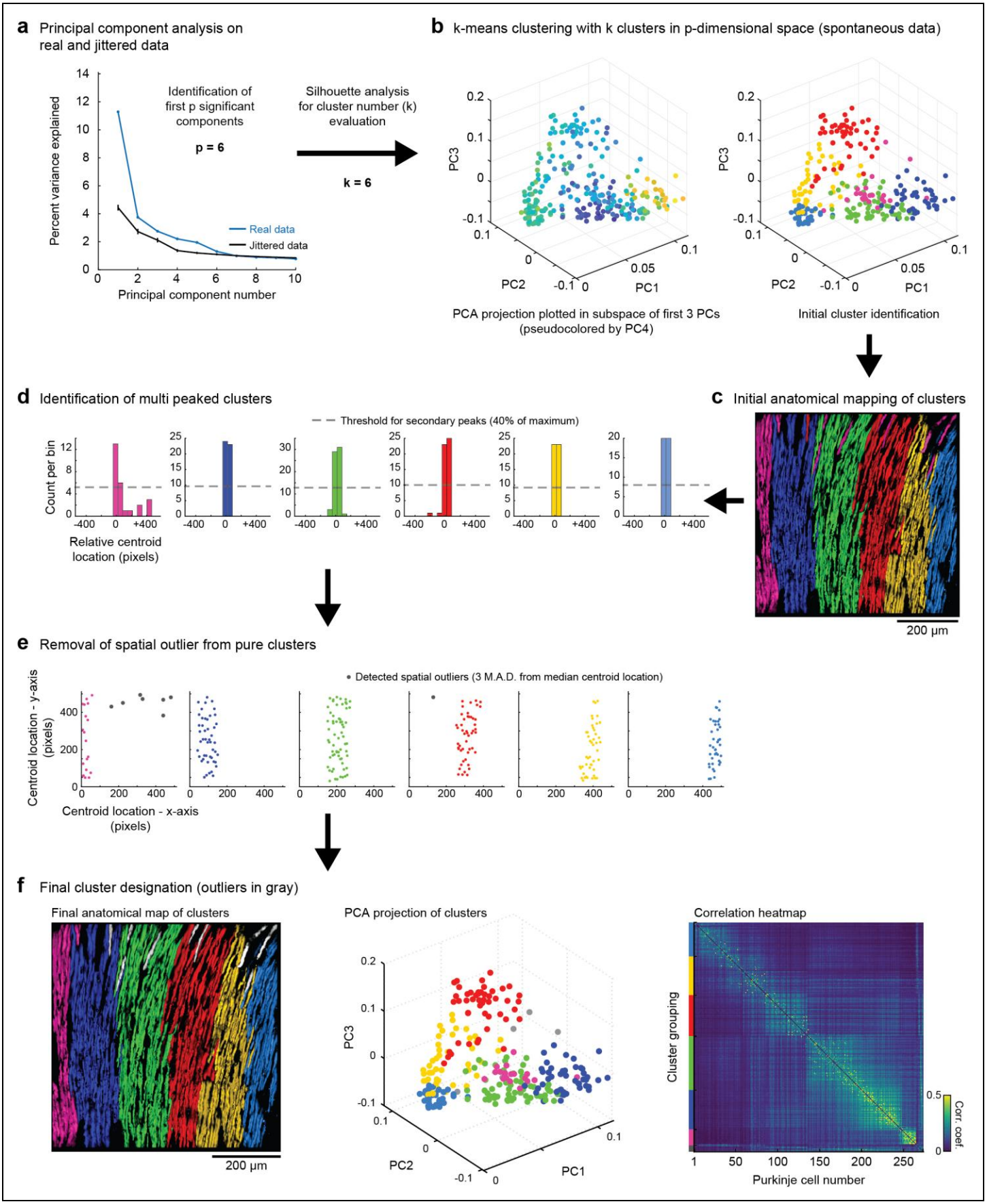
a Principal component analysis on real and jittered data
Identification of first p significant components
p = 6
Silhouette analysis for cluster number (k) evaluation
k = 6
Percent variance explained
Principal component number
Real data
Jittered data
b k-means clustering with k clusters in p-dimensional space (spontaneous data)
PC1
PC2
PC3
PCA projection plotted in subspace of first 3 PCs (pseudocolored by PC4)
Initial cluster identification
c Initial anatomical mapping of clusters
200 µm
d Identification of multi peaked clusters
Threshold for secondary peaks (40% of maximum)
Count per bin
Relative centroid location (pixels)
e Removal of spatial outlier from pure clusters
Detected spatial outliers (3 M.A.D. from median centroid location)
Centroid location - y-axis (pixels)
Centroid location - x-axis (pixels)
f Final cluster designation (outliers in gray)
Final anatomical map of clusters
200 µm
PCA projection of clusters
Correlation heatmap
Cluster grouping
Purkinje cell number
Corr. coef.

Supplementary Figure 2

PCA-based clustering reveals correlated groups of Purkinje cell dendrites

Workflow for microzone identification is shown:

a. Significant principal components were identified by performing 1000 iterations of PCA on cell-wise jittered data (interval ± 400 ms, whole recording) and choosing first p principal components that explained significantly more variance than the jittered components.

b. The appropriate number of clusters for each data set (spontaneous data only) were chosen from the interval [1:12] based on silhouette analysis. PCA projection in 3 dimensions shown before clustering (left, pseudocolored by coefficients of 4th component) and after initial clustering (right, colored by cluster).

c. The initial clusters for each recording were mapped on anatomy and exclusion criteria were applied to obtain pure clusters.

d. ROI centroids were projected on to the mediolateral anatomical axis and binned at ~80 um (64 pixels). Secondary peaks were identified with a threshold of 40% of the maximum bin. If secondary peaks were found, individual ROIs were assigned to the closest peak (none found in example dataset).

e. The median position for each cluster was computed and ROIs that were more than 3 median absolute deviations away from median were excluded as outliers.

f. Final cluster designations were assigned, ROIs were organized spatially within each cluster and clusters were organized spatially relative to each other.

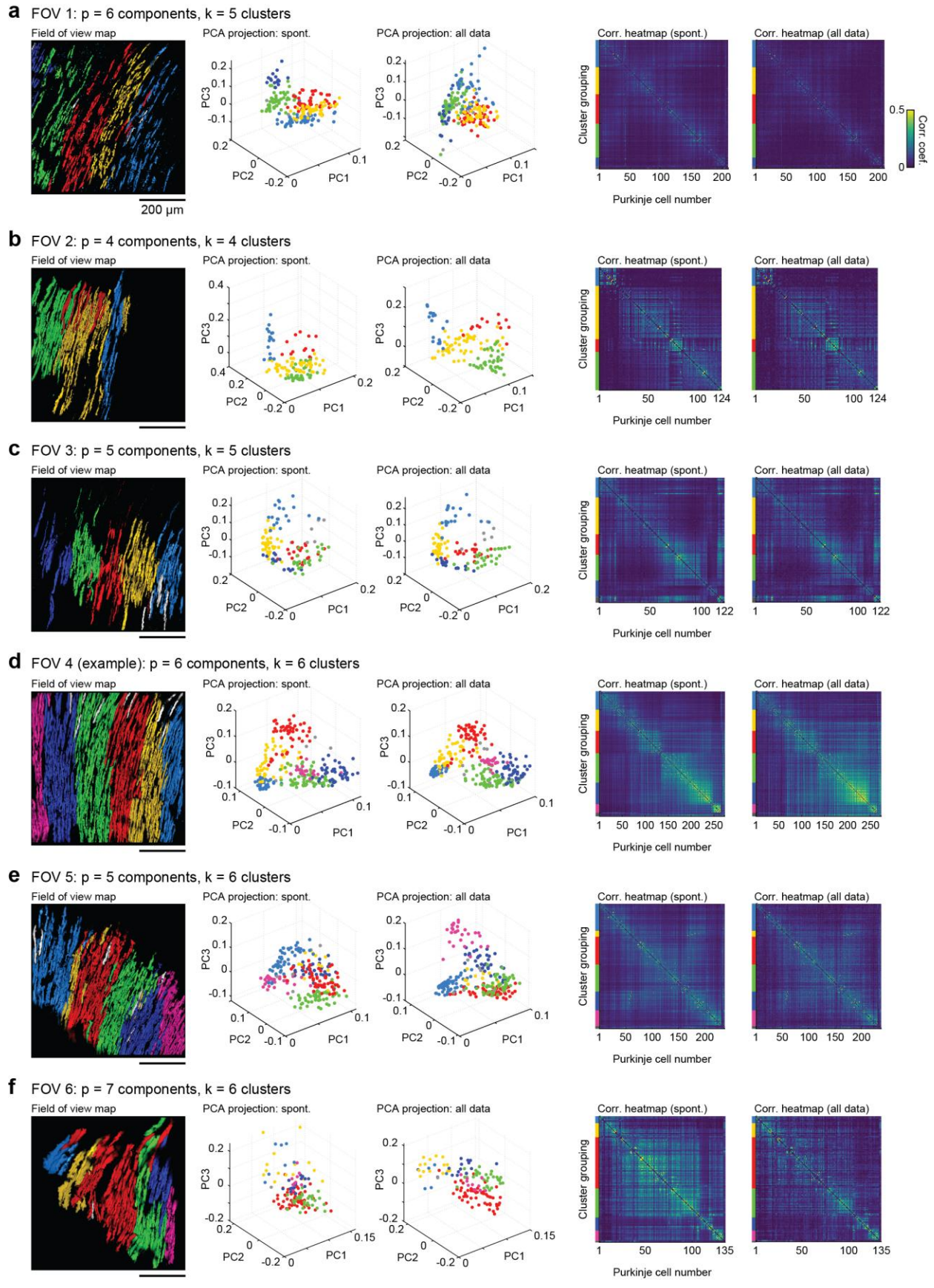
a
FOV 1: p = 6 components, k = 5 clusters
Field of view map
PCA projection: spont.
PCA projection: all data
Corr. heatmap (spont.)
Corr. heatmap (all data)
200 µm
b
FOV 2: p = 4 components, k = 4 clusters
c
FOV 3: p = 5 components, k = 5 clusters
d
FOV 4 (example): p = 6 components, k = 6 clusters
e
FOV 5: p = 5 components, k = 6 clusters
f
FOV 6: p = 7 components, k = 6 clusters
PC1
PC2
PC3
Cluster grouping
Purkinje cell number
Corr. coef.

Supplementary Figure 3

Microzonal identification for each recorded dataset

Anatomical maps (subpanel 1), clustering (subpanels 2 and 3), and correlation heatmaps (subpanels 4 and 5) for fields of view used in Figures 1 – 2. Analysis was done independently for spontaneous activity acquired during withhold periods (spont.) and for whole recording session (all data). Numbers of neurons for fields of view in panels **a**-**f** = 210, 124, 122, 273, 237, and 135, respectively.

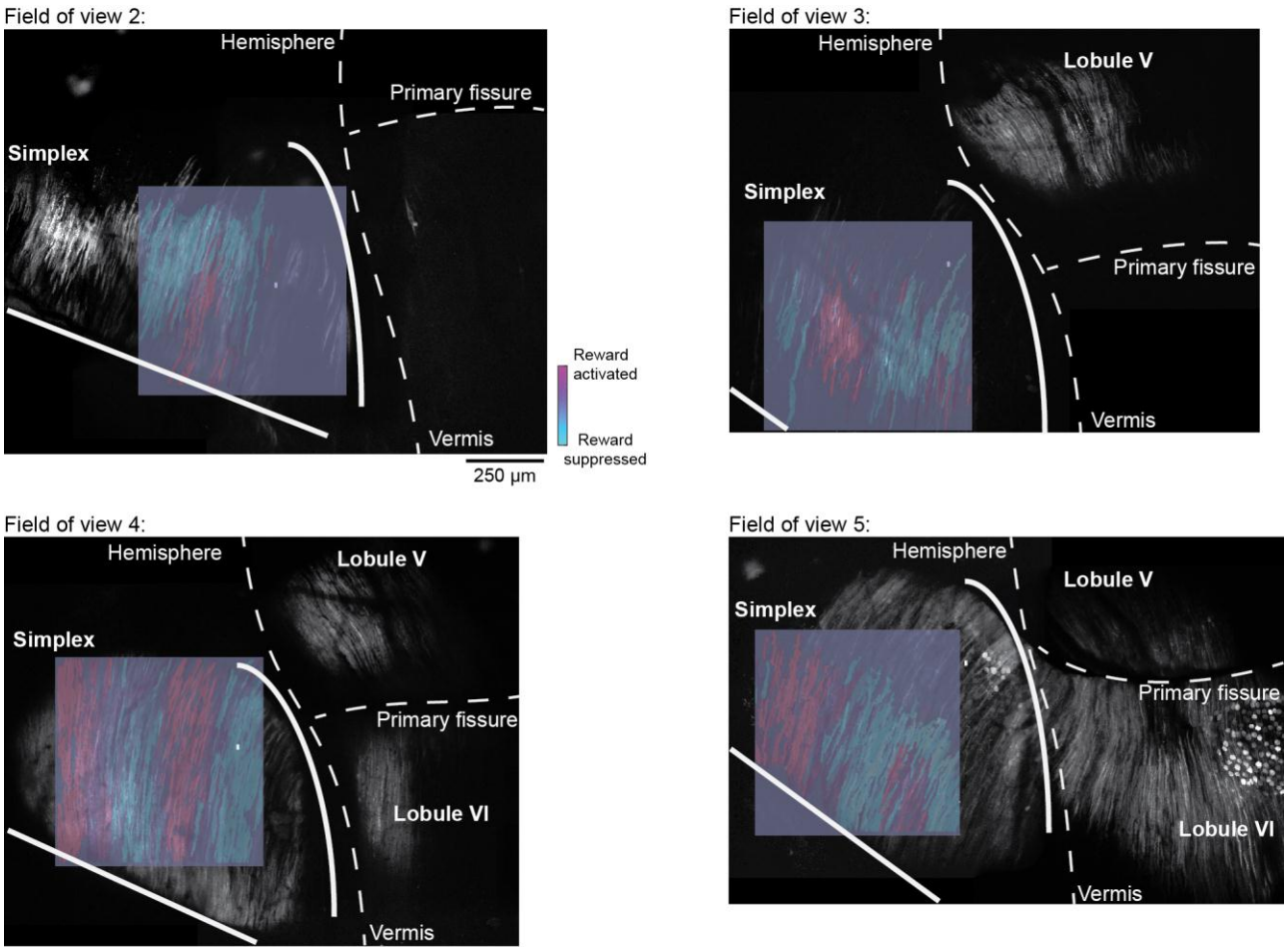

Supplementary Figure 4

Mapping recorded fields of view onto cerebellar anatomy

Coarse anatomical maps with landmarks are shown in grayscale and reward response is shown in color. Field of view number corresponds to numbers given in Supplementary Figure 3. Purkinje cell dendrites with high reward activity (’reward-activated’) are shown in magenta, and Purkinje cell dendrites with low reward activity (’reward-suppressed’) are shown in cyan. Number of trial rewards per field of view: 120 (Field of view 2), 143 (Field of view 3), 156 (Field of view 4), and 52 (Field of view 5).

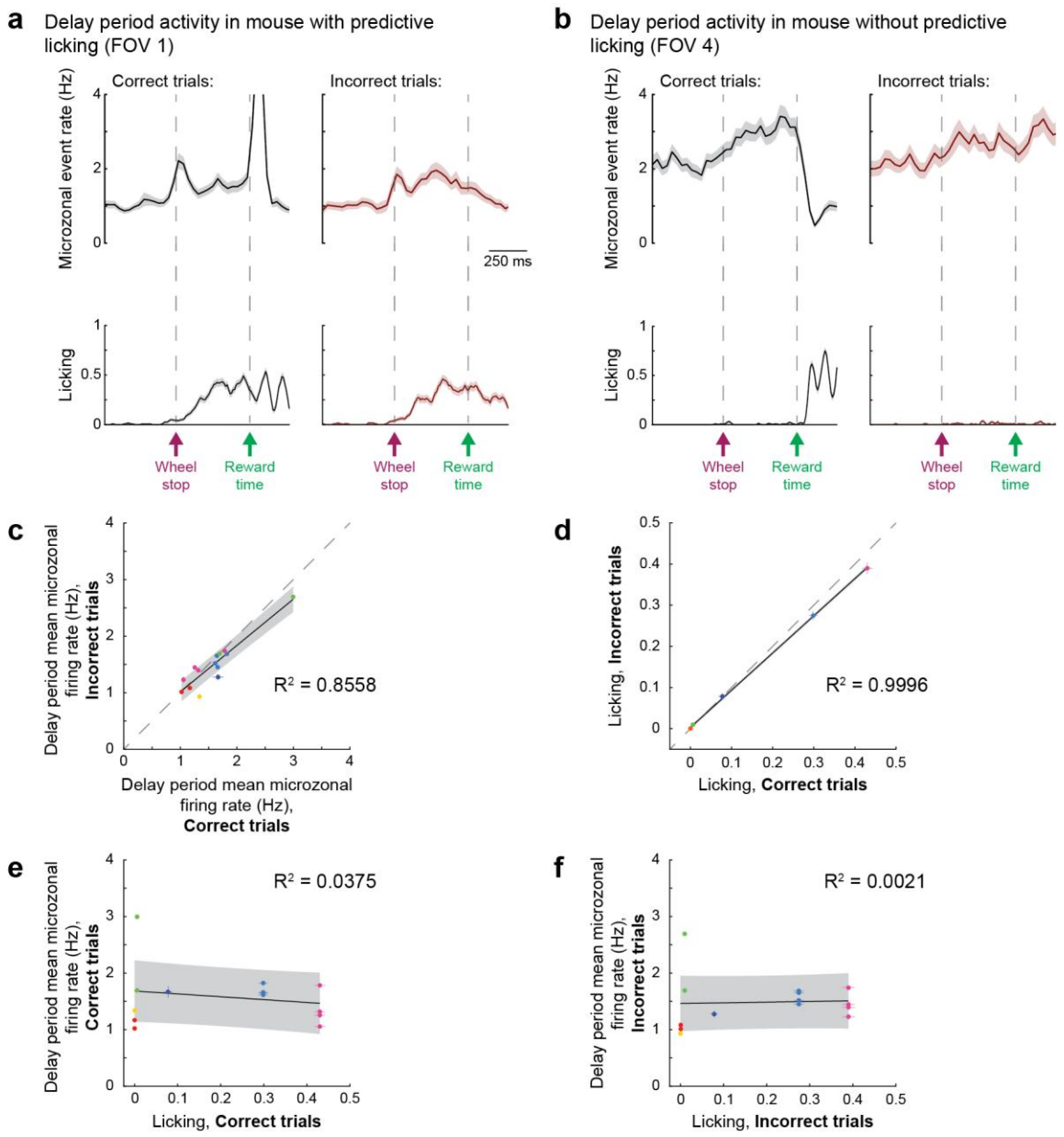

Supplementary Figure 5

Relationship between delay-period activity and predictive licking on operant trials

a. Example of microzone from animal that exhibited predictive licking showing delay period activity on both correct (left, black) and incorrect (right, red) trials. N = 162 correct trials and 124 incorrect trials.

b. Same as panel **a** but for animal that did not exhibit predictive licking. N = 156 correct trials and 115 incorrect trials.

c. Comparison of mean microzonal activity during delay period (-500 to 0 ms relative to reward) in significantly activated microzones on correct and incorrect trials. Dots of the same color represent microzones from the same recording. N = 14 microzones from 6 mice.

d. Comparison of degree of predictive licking on correct and incorrect trials. N = 6 sessions from 6 mice.

e. Relationship between level of delay period activation and degree of predictive licking on correct trials. N = 14 microzones from 6

mice.

f. Same as panel **e** but for incorrect trials.

Traces in panels **a** and **b** and data points in panels **d**-**f** are shown as mean ± s.e.m. Black line and shaded bars in panels **d**-**f** represent linear fit and 95% confidence interval through all data points (linear regression; panel **c**, $p = 2x10^{-6}$; panel **d**, $p = 5x10^{-8}$; panel **e**, $p = 0.5$; panel **f**, $p = 0.9$).

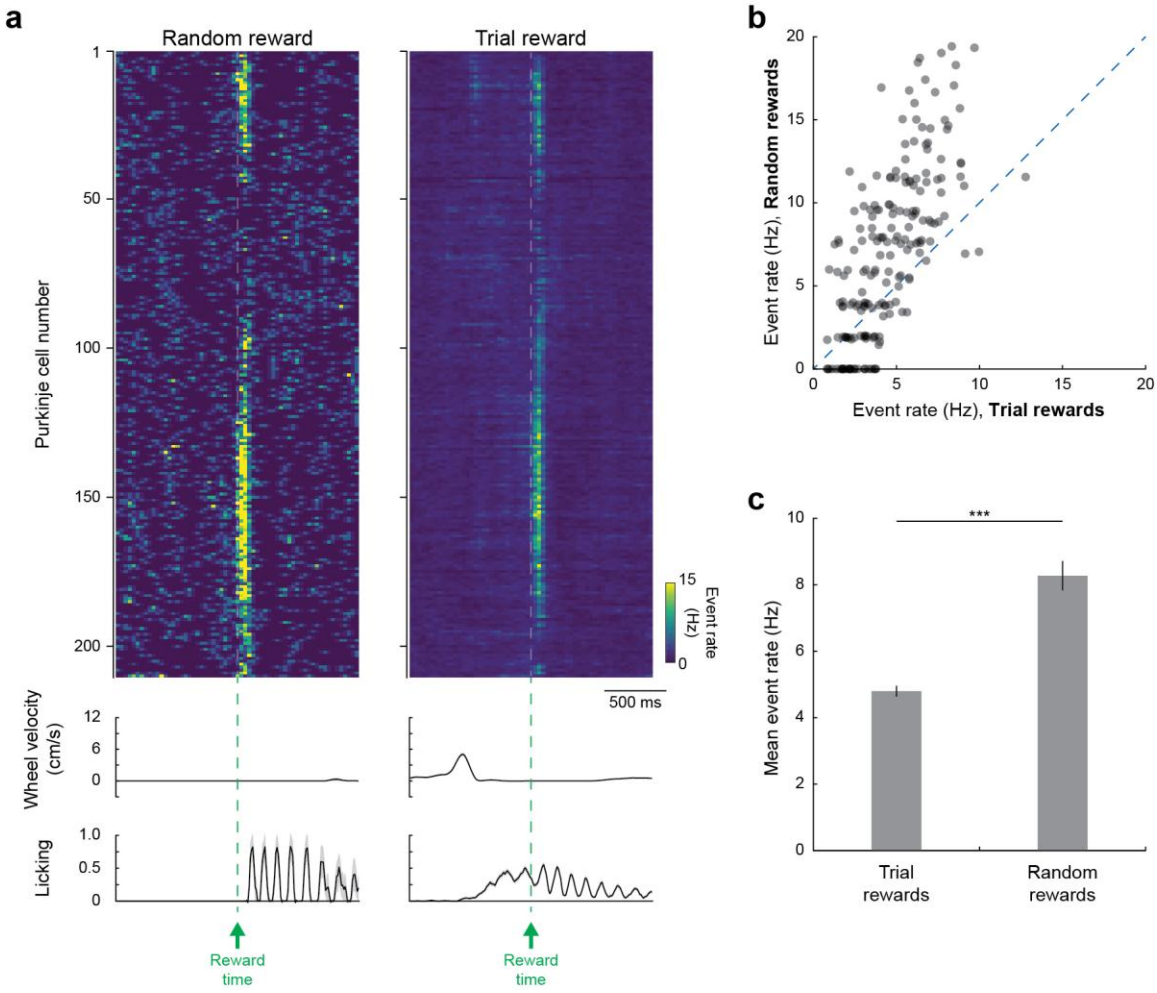

Supplementary Figure 6

Initial observation of reward-response modulation

a. Top: Trial-averaged population response in the first mouse in which we observed reward response modulation (Supplemental Figure 3, FOV 1). Middle: Trial-averaged steering wheel velocity. Bottom: Trial-averaged licking response. Data are shown as mean ± s.e.m. across trials (n = 162 trial rewards and 5 random rewards). In this experiment, the mouse was not subjected to all of the potential reward contingencies, only to random and trial-dependent (operant) rewards, but still exhibited the characteristic reward response modulation.

b. Scatter plot comparing reward-related responses over interval 0 to +100 ms post reward for random rewards and rewards earned on correct motor trials.

c. Cell-wise average of Purkinje cell dendritic response to trial rewards and random rewards taken over interval 0 to +100 ms post reward. Data are shown as mean ± s.e.m. across cells (n = 210 cells, two-sided Wilcoxon signed-rank test, $p = 3x10^{-18}$).

Statistics summary: ***$p < 0.001$.

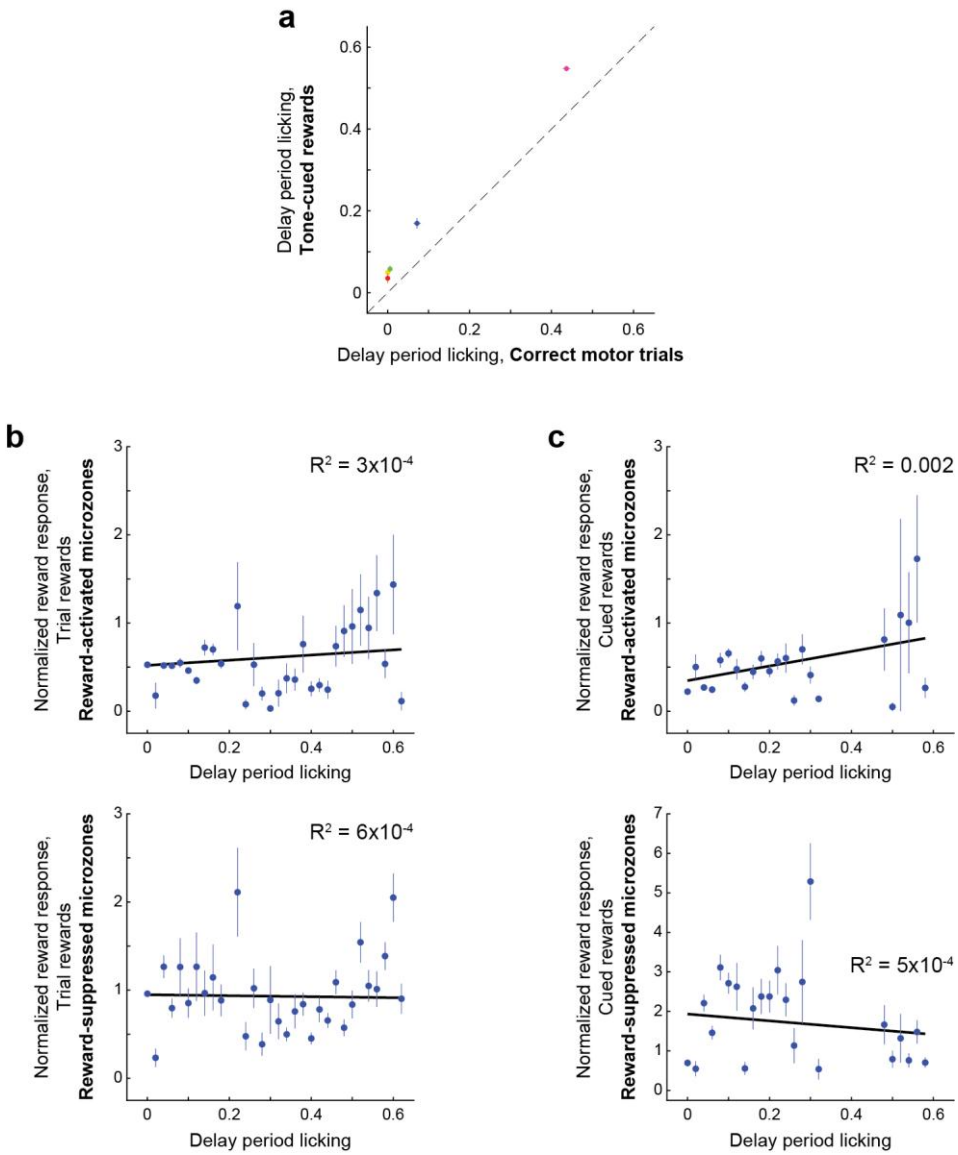

Supplementary Figure 7

Quantification of licking responses across reward conditions

a. Comparison of delay period (reward-predictive) licking for tone-cued rewards and correct motor trials (-500 to 0 ms relative to reward in both conditions, which had the same delay interval). Mean licking responses in individual mice (n = 5) are as single colored dots with error bars showing across trial s.e.m. All mice exhibited higher predictive licking for tone-cued rewards than on correct motor trials ($p = 3x10^{-22}$ (Mouse 1, yellow), $p = 5x10^{-17}$ (Mouse 2, red), $p = 1x10^{-16}$ (Mouse 3, green), $p = 1x10^{-7}$ (Mouse 4, blue), $p = 1x10^{-6}$ (Mouse 5, magenta), two-sided Wilcoxon rank sum test across trials).

b. Normalized response to trial rewards (mean activity in interval 0 to +100 ms after reward in Purkinje cells from reward-activated microzones (top) and reward-suppressed microzones (bottom) as a function of degree of predictive licking. Reward-related responses and predictive licking were quantified on individual trials, after which responses in individual neurons were normalized to the mean response to random reward per neuron and all neuron-trial pairs were binned for plotting according level of predictive licking in each trial.

c. Same as panel a but for cued rewards.

Data are shown as mean ± s.e.m. In panels **b** and **c**, N = 38337 neuron-condition pairs (trial rewards, activated), 51888 pairs (trial rewards, suppressed), 11584 pairs (cued rewards, activated), and 11314 pairs (cued rewards, suppressed). The number of Purkinje cells = 361 (reward-activated) and 450 (reward-suppressed) pooled from 5 mice. Black line represents linear fit through all data points (not binned).

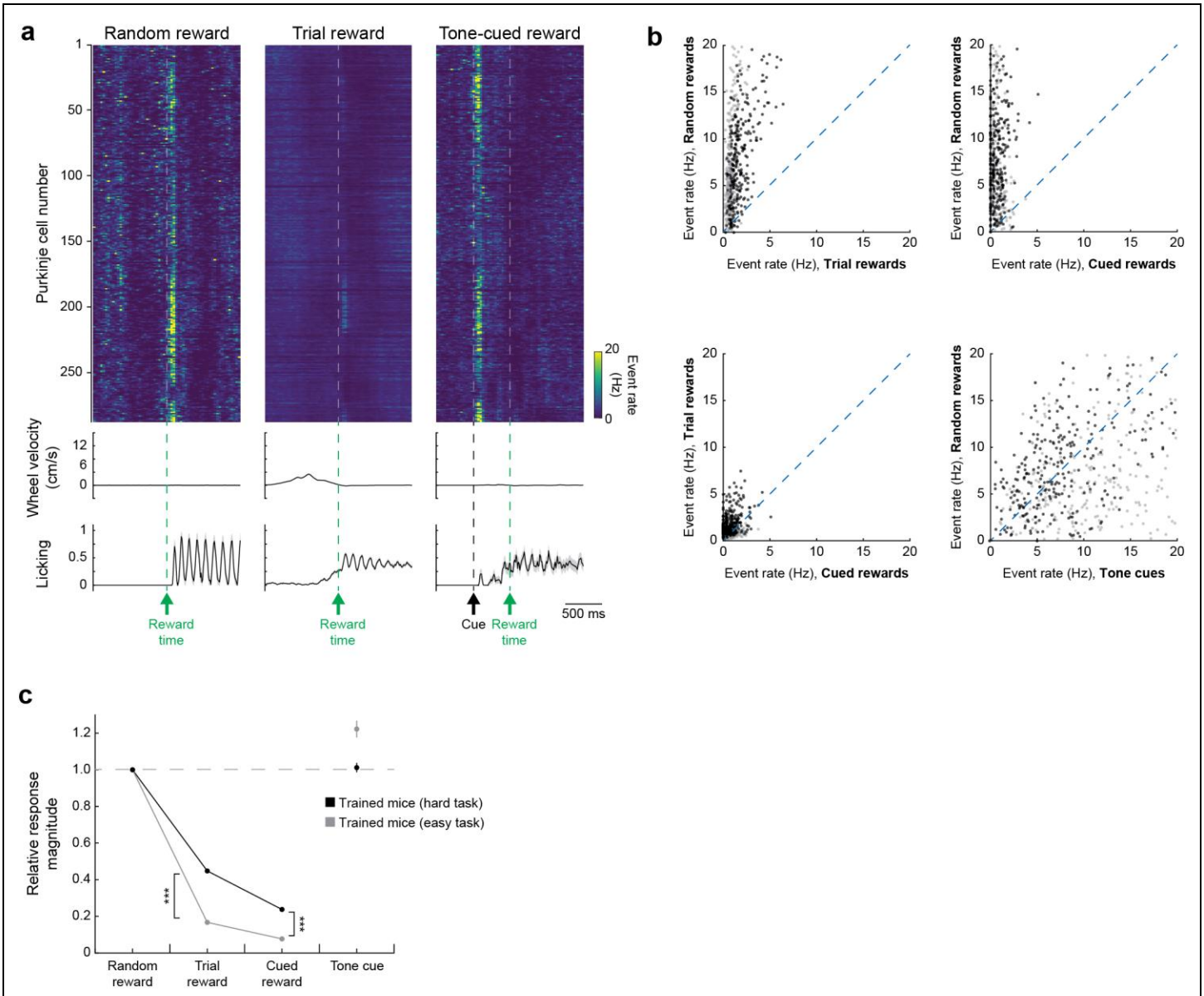

Supplementary Figure 8

Stronger suppression of reward response on operant trials with an easier task

a. Top: Trial-averaged population response of a representative field of view to random, operant, and tone-cued rewards on a different task version in which all wheel movements towards the midline were rewarded. ROIs are by mediolateral position within the field of view. Middle: Trial-averaged steering wheel velocity. Bottom: Trial-averaged licking response. Velocity and licking are shown as mean ± s.e.m. across trials (n = 11 random rewards, 210 trial rewards, and 20 tone-cued rewards).

b. Scatter plots showing pairwise comparisons of response amplitude (computed as mean over 0 to +100 ms after each reward-related event) across different reward conditions. N = 556 neurons from 2 FOVs in 2 mice. Data points from representative field of view (panel **a**) are shown in darker gray.

g. Relative response magnitude in neurons responsive to random reward (mean response over 0 to 100 ms after random reward > 2 s.d. above baseline) in mice trained on the task used throughout the majority of this study (black) and the easier task version (gray). Data are shown as mean ± s.e.m., and n = 400 neurons (of 891) for mice trained on the hard task and n = 417 neurons (of 556) for mice trained on the easy task (Kruskal-Wallis test, H = 2543, d.f. = 7, $p < 1x10^{-99}$, significance values for Bonferroni-corrected individual

comparisons: hard task vs easy task (trial reward), $p = 5x10^{-25}$; hard task vs easy task (cued reward), $p = 9x10^{-15}$).

Statistics summary: ***$p < 0.001$.

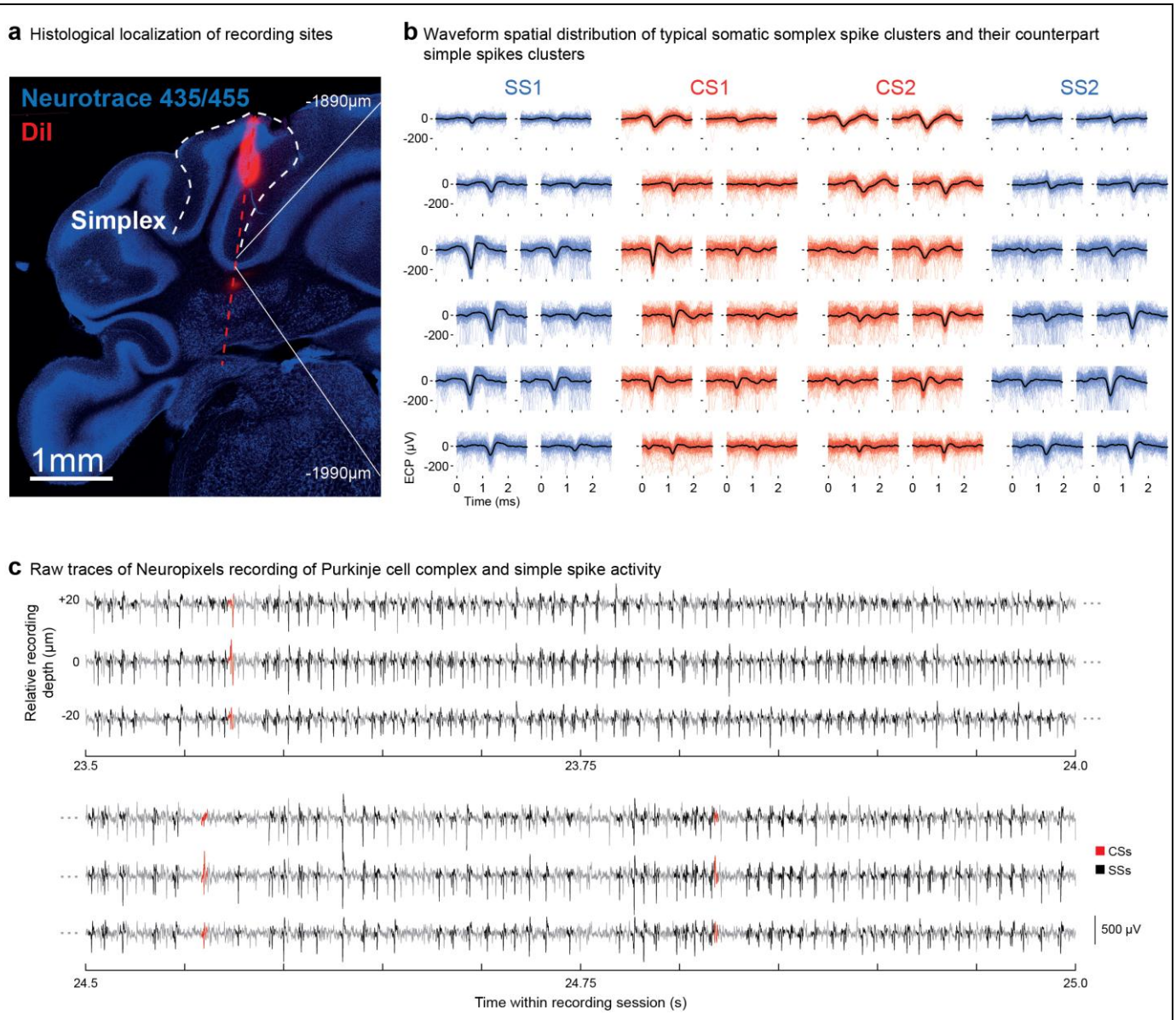

Supplementary Figure 9

Recordings from Purkinje cells using Neuropixels probes

a. Histological localization of the Neuropixels recording track in a coronal section of cerebellum (6.2mm caudal from bregma). Blue: Neurotrace, Red: DiI (highlighting the electrode track). Dashed red line shows the projection of the electrode track onto this anatomical section.

b. Examples of complex spikes (CSs) and simple spikes (SSs) recorded using Neuropixels probes. Each panel shows 100 overlaid raw traces (with mean and s.d. shown as black line and shaded area, respectively) on adjacent recording sites (20 µm vertical and horizontal separation), situated from -1890 µm to -1990 µm below the surface of the brain shown in panel **a**. Red: CS recordings showing channels located in the molecular (top channels) and Purkinje (middle channels) layers of the cerebellar cortex. Blue: corresponding SS recordings from the same putative Purkinje cells exhibiting post-CS pauses, as in Figure 4C (SS1 and SS2 associated with CS1 and CS2, respectively).

c. Example raw traces (gray) recorded on three adjacent vertically consecutive channels (20 µm separation) of a Neuropixels probe within the Purkinje cell layer. The spikes of the simple spike cluster (black) and complex spike cluster (red) shown in Figure 4A-C are

highlighted. Note that several other simple and complex spike clusters were identified within this Purkinje cell layer but are not highlighted for clarity.

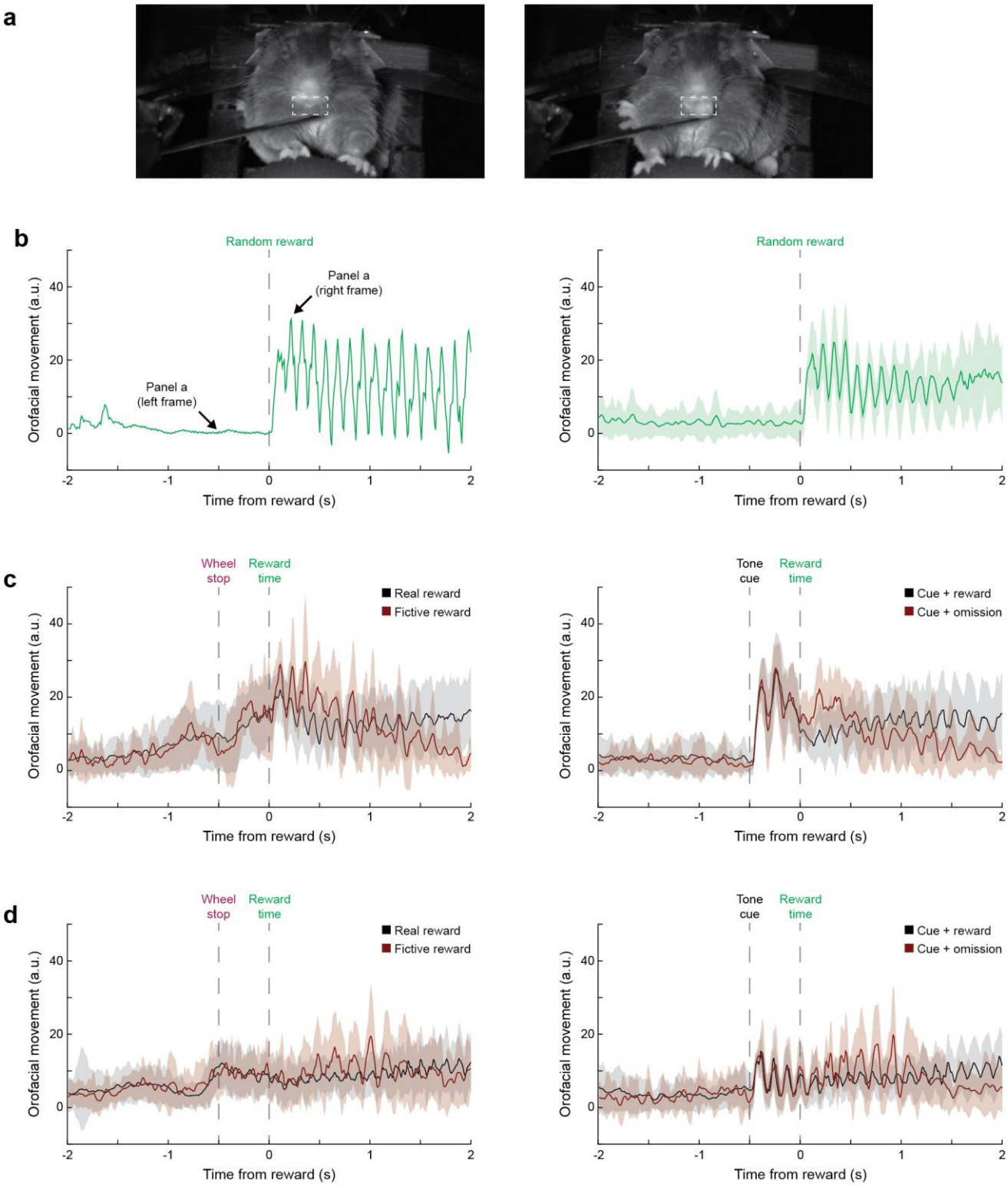

Supplementary Figure 10

Video analysis of orofacial movements on omission trials

To better understand how complex spiking responses upon reward omission might be reflected behaviorally, we analyzed videos of orofacial movements in a subset of mice presented with real and fictive trial reward and with delivered and omitted cued rewards. We observed that upon violations of reward expectations, mice exhibited larger orofacial movements, consistent with them searching for an expected reward.

a. Two video frames (taken at 100 Hz) show mouse 500 ms before a random reward was delivered (left) and 220 ms after the random reward was delivered (right). White dashed boxes indicate regions of analysis (~4 x 8 mm).

b. Orofacial movement signal recorded for a single random reward (left, corresponding to video frames in panel **a**) and the mean orofacial movement signal (right) across all random rewards in a session (n = 30).

c. Mean orofacial movement signals from example mouse (same session as panels **a** and **b**) on operant trials (left) with real reward (black, n = 52) and fictive reward (red, n = 8), and signals on cued reward trials (right) on which reward was given (black, n = 40) and omitted (red, n = 14).

d. Same as panel **c** but for a different mouse. N = 54 operant trials with real reward, 14 operant trials with fictive reward, 53 cue + reward trials, and 12 cue + omission trials.

Data in panels **b** - **d** are shown as mean ± s.d. across trials.

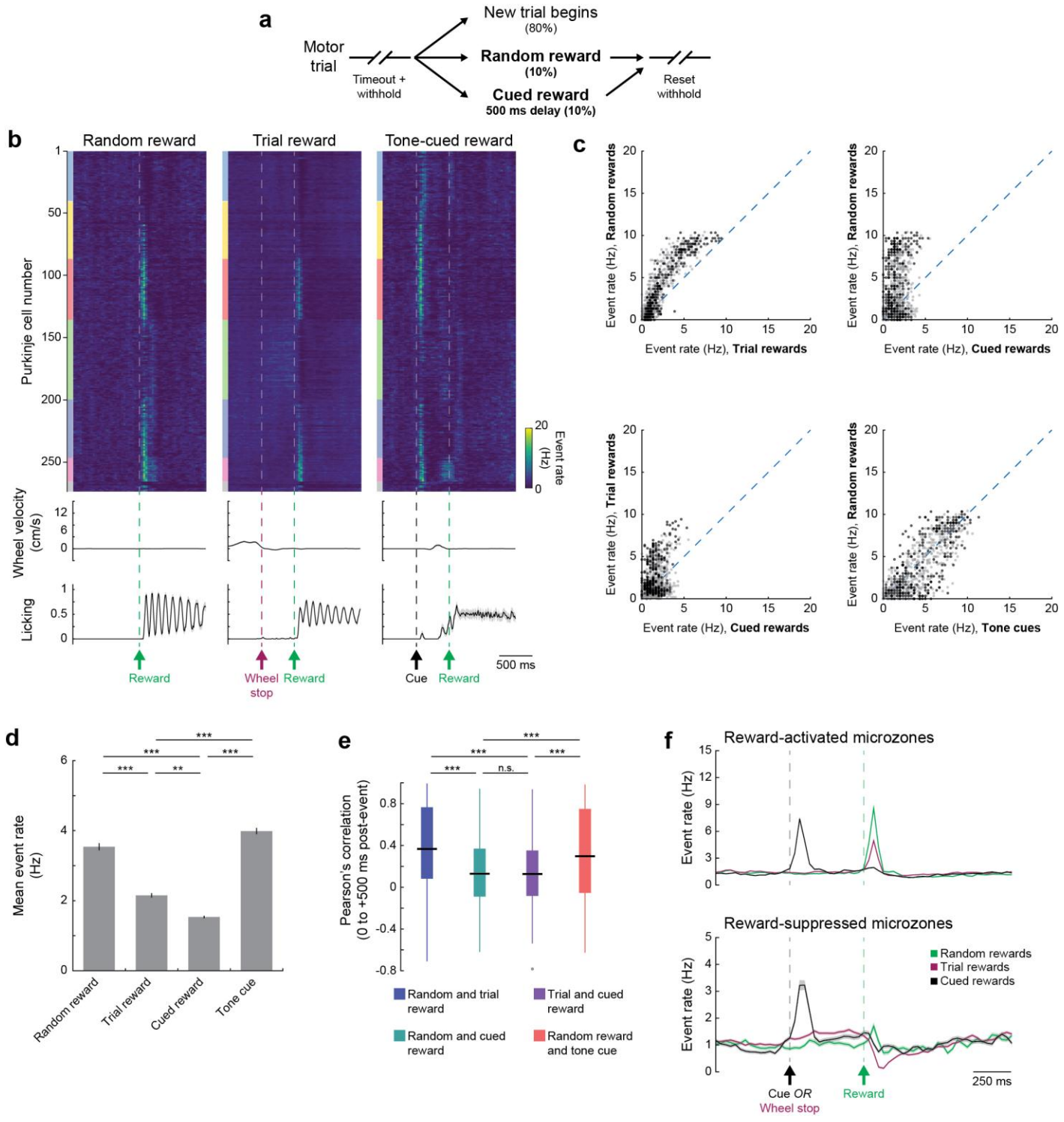

Supplementary Figure 11

Modulation of reward responses calculated using unweighted event detection

Data used in this figure are the same as in Figure 3 of the main text, but all detected event amplitudes are set to a value of 1.

a. Schematic of reward perturbation experiments: during each behavioral session, we randomly interspersed random rewards (10% of inter-trial intervals) or tone-cued rewards (also 10% of inter-trial intervals; 500 ms delay between cue onset and reward).

b. Top: Trial-averaged population response of a representative field of view (same as Figure 2) to random, operant, and tone-cued rewards. Dendritic calcium event matrix was binarized for this analysis, setting all event amplitudes to a value of 1. ROIs are sort first by medio-lateral position of identified microzones, then mediolaterally within each identified microzone. Color blocks adjacent to each heatmap denote microzonal designation, following the color scheme of Figure 2 (gray = unclustered). Middle: Trial-averaged steering wheel velocity. Bottom: Trial-averaged licking response. Velocity and licking are shown as mean ± s.e.m. across trials. N = 30 random rewards, 156 trial rewards, and 30 tone-cued rewards.

c. Scatter plots showing pairwise comparisons of response amplitude (computed as mean over 0 to +100 ms after each reward-related event) across different reward conditions. N = 891 neurons from 5 FOVs in 5 mice. Data points from representative field of view (panel **b**) are shown in darker gray.

d. Cell-wise average of Purkinje cell dendritic response to each reward-related event. Data are shown as mean ± s.e.m. (n = 891 neurons from 5 FOVs in 5 mice, Kruskal-Wallis test, H = 428, d.f. = 3, $p = 2x10^{-92}$, significance values for Bonferroni-corrected individual comparisons: random vs trial reward, $p = 4x10^{-17}$; random vs cued reward, $p = 1x10^{-32}$; trial vs cued reward, p = 0.004; trial reward vs tone cue, $p = 1x10^{-51}$; cued reward vs tone cue, $p = 4x10^{-77}$).

e. Cell-wise comparison of Pearson's correlations between pairs of reward-related events computed over 0 to +500 ms after each event. Data are shown as box plots: center line, median; box edges, interquartile ranges; whiskers, range without outliers (1.5 times the interquartile range from box edges); gray points, outliers (n = 891 neurons from 5 FOVs in 5 mice, Kruskal-Wallis test, H = 245, d.f. = 3, $p = 8x10^{-53}$, significance values for Bonferroni-corrected individual comparisons: random and trial reward vs random and cued reward, $p = 1x10^{-34}$; random and trial reward vs trial and cued reward, $p = 6x10^{-37}$; random and cued reward vs trial and cued reward, p > 0.9; random and cued reward vs random reward and tone cue, $p = 5x10^{-17}$; trial and cued rewards vs random reward and tone cue, $p = 1x10^{-18}$).

f. Time course of mean responses across reward conditions for Purkinje cells in reward-activated microzones (top, n = 361 neurons) and reward-suppressed microzones (bottom, n = 470 neurons). Note that 60 neurons were not clustered into a microzone and so excluded from this analysis. Data are shown as mean ± s.e.m.

Statistics summary: n.s. = not significant, **p < 0.01, ***p < 0.001.